High-contrast, high-resolution photochromic silicone polymer based on photoswitchable $[Ru(bpy)_2OSO]PF_6$ building blocks

Kristin Springfeld,* Volker Dieckmann, and Mirco Imlau

Department of Physics, Osnabrück University, Barbarastraße 7, 49076 Osnabrück, Germany
**Corresponding author: kspringf@uos.de*

Received July 19, 2013; revised September 6, 2013; accepted September 7, 2013;
posted September 10, 2013 (Doc. ID 194127); published November 19, 2013

The implementation of photoinduced linkage isomerism in molecular-based optical materials represents a promising approach for the synthesis of high-contrast, high-resolution photosensitive materials that are necessary for high-density (holographic) data storage and/or real-three-dimensional (holographic) displays. The unsolved task of embedding a photofunctional coordination complex into a matrix like polymer polydimethylsiloxane (PDMS) with photoinduced isomerism of a SO-bond in the sulfoxide compound $[Ru(bpy)_2OSO]PF_6$ is addressed. This approach allows to preserve the spectral properties within the solid dielectric environment, with an impact of PDMS on population and relaxation dynamics. All data are discussed in the framework of photofunctionality, storage, and display applications.

OCIS codes: (210.0210) Optical data storage; (090.2870) Holographic display; (090.2900) Optical storage materials; (160.5335) Photosensitive materials; (160.5470) Polymers.
http://dx.doi.org/10.1364/PRJ.1.000197

1. INTRODUCTION

The combination of nanoscaled, photofunctional building blocks to complex functional materials with macroscopic effects represents a crucial step toward applications of the next generation in nonlinear optics and photonics. A prominent example is optical materials built from small photoswitchable coordination compounds [1]. The photo-physics and -chemistry of the relevant molecular classes have been studied comprehensively on the molecular level in recent decades. Their immense potential for the control of light by light is ascribed to their intrinsic photofunctionality of photoinduced refractive-index changes on the molecular level, which has been demonstrated as a general property of coordination compounds featuring photoinduced linkage isomerism [2]. Recording of dynamic, high-resolution Bragg gratings with diffraction efficiencies of more than 90% in a 200 μm thick sample was successfully demonstrated [3], which exceeds the properties of classical photorefractive materials by one order of magnitude for the same thickness [4]. Apparently, a three-dimensional (3D) matrix of small photoswitchable coordination compounds is the key for visionary applications like real-time, three-dimensional holographic displays [5] or optical and holographic data storage [6,7].

However, the combination of these molecules and bulky media with appropriate macroscopic function (see, e.g., [8]) and optical quality is to be solved. The most prominent state-of-the-art strategies are as follows: (i) Single crystal growth from aqueous solutions [9]. This enabled structural analysis of photoinduced linkage isomerism by means of x ray [10] or neutron diffractometry [11] in photocrystallography [12,13]. (ii) Linkage of functional molecules to a polymeric side [14–17] with the obvious advantage of the huge density of the compounds within the polymer [18]. (iii) Electrostatic attachment to charged anchors (without losing the photofunctionality [19]). (iv) Embedding into a nanostructured matrix, for instance into mesopores of xerogels [20]. Further strategies are required if the costs of chemical synthesis; the stability of photofunctionality on the long term; and the synthesis of homogeneous, bulky media with large dimensions, as well as a sufficient transmission and low density of scattering centers, must be considered for the case of applications.

In this contribution, we present photochromic silicone polymers based on the coordination compound $[Ru(bpy)_2OSO]PF_6$ (OSO) from the class of ruthenium sulfoxides [21]. Its photophysics is characterized by a photoinduced linkage isomerization from an S- to O-bonded Ru atom [22]. Already, it has been demonstrated with solutions of OSO in dichloromethane (DCM) that these compounds facilitate the essential requirements such as high sensitivity, pronounced photorefractive properties, and a high spatial resolution for use in the new photonic devices [8]. Here, solid-state materials of OSO were prepared by embedding it into dielectric polydimethylsiloxane (PDMS). PDMS offers a high transmission of $T > 80\%$ in the visible/NIR spectral range. Furthermore, it is temperature-stable ($-50°C < T < +200°C$), inexpensive, and nontoxic and provides a high chemical stability. With these OSO compounds embedded in PDMS, we first addressed the question whether the solid dielectric environment has an impact on the principle photofunctionality of the compounds. For this purpose the steady-state and light-induced absorption were measured and compared with the results obtained for OSO in a DCM solution. Particularly the dynamics of both population and thermal decay are affected significantly, while the spectral fingerprints show only slight modifications. Second,

we focused on the impact of photochromic silicone polymers for image and/or hologram recording. Thus, optical homogeneity of the sample prior to and after light exposure as well as dynamic range and spatial resolution of recorded test images were investigated. We discuss these results in the framework of visionary applications of modern optical holography.

2. RESULTS AND DISCUSSION

Figure 1 shows a solid-state sample of the OSO compound embedded into PDMS with dimensions of 24.5 mm × 24.5 mm × 1.5 mm. For comparison, the commonly prepared solution of OSO in DCM filled into an optical cuvette with equivalent molar concentration $c = (0.3 \pm 0.1)$ mM is shown.

The typical yellow color of the samples originates from a broad extinction feature centered at about 25,000 cm^{-1} (cf. extinction spectra in Fig. 2), that is related to the Ru$d\pi\rightarrow$bpy π^* metal to ligand charge transition (MLCT) transition [23]. Further prominent extinction features in the UV range at about 35,000 cm^{-1} have been assigned to intraligand transitions at the bpy rings [24].

Both bands appear to be slightly modified in the PDMS sample, which can be analyzed qualitatively from the mathematical adaptation of the extinction bands using an appropriate combination of Voigt and Gaussian profiles (gray lines) [22]: the amplitude of the MLCT band increases by about 5% together with a blueshift of the central wavenumber by 900 cm^{-1} to $\nu = 25{,}500$ cm^{-1} (392 nm) in PDMS. At the same time the intensity of the extinction band of the ligand centered (LC) transition in the UV range is reduced by about 15%. Its position is redshifted by about 500 cm^{-1} to 34,600 cm^{-1}. Both absorption features show a pronounced line broadening of more than 30% in comparison to the OSO solution. All these modifications in the ground-state spectra can be attributed to the influence of the exchanged environment from DCM to PDMS that differs with respect to the respective polarity and viscosity [25].

Figures 3(a) and 3(b) verify the photofunctionality of the solid-state sample: Its extinction characteristics are plotted as a function of time ($0\ \text{s} < t < 10{,}000$ s) when exposed to a standard white light source ($400 < \lambda < 800$ nm, average intensity $I_{wl} \approx 25$ mW cm^{-2}) both via the extinction spectra $\varepsilon(\lambda)$

Fig. 1. Solid-state sample of OSO embedded in PDMS (left) and the commonly studied solution of OSO in DCM in a cuvette (right).

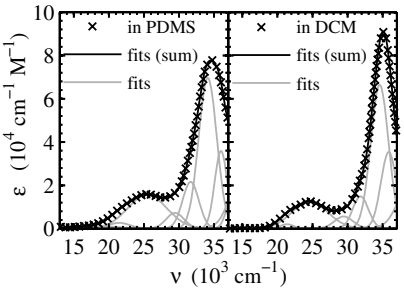

Fig. 2. Extinction spectra $\varepsilon(\nu) = \alpha(\nu)/c$ of OSO embedded in PDMS (left) compared to a solution of OSO in DCM (right), modeled by a sum of Voigt and Gaussian profiles [22].

in the UV/visible/NIR range [Fig. 3(a)] and via the normalized extinction change $\delta\varepsilon$ at $\lambda = 500$ nm [Fig. 3(b)].

The spectra of the exposed PDMS sample show the buildup of two broad extinction bands at $\lambda = 355$ nm and $\lambda = 504$ nm, as has been established for OSO solutions in DCM [22,26]. Unambiguously, these extinction features originate from photoinduced linkage isomerization of the OSO compound as the pronounced extinction band related to the MLCT likewise vanishes and there are three isosbestic points at $\lambda = 331$ nm, $\lambda = 386$ nm, and $\lambda = 444$ nm; that is, it is a reaction of the first order. As a remarkable characteristic of the solid-state sample, its population dynamics of the linkage isomerization process during light exposure are slowed down. A fit of a two-fold exponential function to the data of Fig. 3(b) [27],

$$\delta\varepsilon_{\text{fit}}(t) = \delta\varepsilon_0 + A_1 \exp\left(-\frac{t}{\tau_1}\right) + A_2 \exp\left(-\frac{t}{\tau_2}\right), \qquad (1)$$

yields the characteristic time constants $\tau_1 = (170 \pm 7)$ s and $\tau_2 = (1000 \pm 50)$ s that are larger by a factor of 10 compared with OSO in propylene carbonate solutions [27]. This can be attributed to the influence of the viscosity of the dielectric environment and is in agreement with [26].

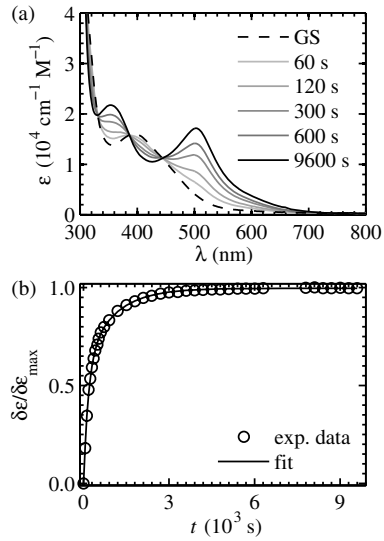

Fig. 3. (a) Extinction characteristics of the OSO-PDMS sample as a function of time when exposed to a white-light source at room temperature. (b) Characteristics of (a) for the experimental data (o) at $\lambda = 500$ nm and the fit according to Eq. (1) (black line).

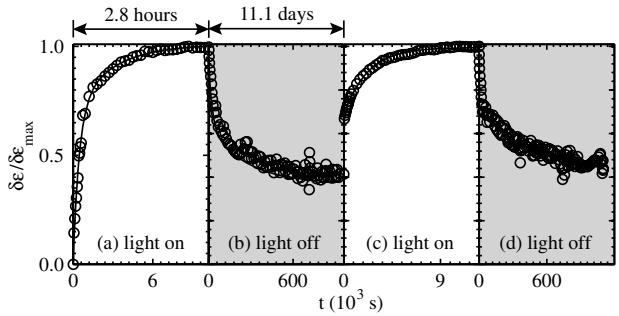

Fig. 4. Double population-thermal relaxation-cycle of the OSO-PDMS sample at $\lambda = 500$ nm: (a) Optical population of the molecules from the ground state into the metastable structural isomers with (b) subsequent thermal relaxation back to the ground state. (c) Afterward, the molecules are transferred back to the metastable states by a second optical excitation. The following thermal relaxation to the ground state is shown in part (d), indicating a reproducible excitation cycle.

Figure 4 shows the temporal dynamics of the thermally activated decay of the molecular isomers back to the ground state.

The data were collected upon saturation of the extinction change being reached by white light exposure at an elevated temperature of $T = 45°C$. Thereby, the dynamics of both the population and the thermal decay are accelerated. This enables the determination of the characteristic decay time constants to $\tau_1 = (2.5 \pm 0.2) \times 10^4$ s and $\tau_2 = (2.7 \pm 0.2) \times 10^5$ s by means of data fitting with a two-fold exponential function. These time constants are larger by a factor of about 100 in comparison to OSO in DCM solution, in which constants of $\tau_1 = (1.6 \pm 0.3) \times 10^3$ s and $\tau_2 = (6.2 \pm 0.1) \times 10^3$ s can be observed. These are equivalent to time constants reported for propylene carbonate solutions in [22]. At the same time, the thermal decay saturates at a value of about 40% of the maximum extinction change; that is, a significant fraction of the OSO isomers are not transferred to their structural ground state. This saturation value is conserved in a second cycle of optical excitation/thermal decay, yielding characteristic time constants in the same order of magnitude as in the first cycle. Thus, it can be concluded that ≈60% of the embedded molecules participate in the photofunctionality of the solid-state sample. The residual molecules become optically inactive after their first isomerization process that underlines the significant impact of the PDMS environment to the energetic potential of the OSO molecules. We like to note that aging of the molecular samples in the dark could not be detected over a duration of 10^7 s; that is, the photofunctionality was not altered for aged solid-state samples. In solutions, enclosure of an argon atmosphere is absolutely required to prevent degradation by air.

Equivalent results on the photofunctionality and impact of PDMS environment were obtained for different OSO compounds embedded in PDMS, such as $[Ru(bpy)_2BnOSO]PF_6$ (BnOSO), $[Ru(bpy)_2BnClOSO]PF_6$ (BnClOSO) and $[Ru(bpy)(biq)OSO]PF_6$ (BIQ). These compounds show different energetic landscapes and, thus, different spectral positions of the MLCT and LC transition bands, due to ligand substitution or the substitution of one of the nonswitching 2,2′-bipyridine rings by a 2,2′-biquinoline (biq) ligand [28]. For instance, the central wavelength of the extinction band of the MLCT in BIQ is redshifted by about 80 nm, [26] so that it becomes possible to synthesize solid state sulfoxides with photosensitivities at different wavelengths.

3. APPLICATIONS

Figure 5(a) shows the spatial homogeneity of the extinction coefficient at $\lambda = 400$ nm (MLCT transition) within an area of ≈27 mm^2 of an as-prepared OSO-PDMS sample.

Variations in the order of ±5% are due to concentration inhomogeneities of the molecular compounds within the PDMS bulk. Then, the spatial distribution of the extinction coefficient was measured again, but at a different wavelength of 500 nm and upon exposure to a white light spot generated by a pinhole ($d = 2.6$ mm) [cf. Fig. 5(b)]. Here, the tremendous dynamic range of the extinction change of about 200% related to the values of the unexposed sample becomes visible. Finally, optical image recording was performed by means of white-light photolithography and applying the emblem of the University of Osnabrück (metallic negative mask) as a test mask. Thereby, the ability for RGB displays is analyzed via photometric characteristics. Figure 6(a) shows a photograph of the recorded image in a transmission-line geometry using a white-light source and a digital photocamera. Thus, the characteristic colors of molecules in the ground state (yellow color due to the extinction feature of the MLCT transition in the blue spectral range) and metastable state (red color due to the

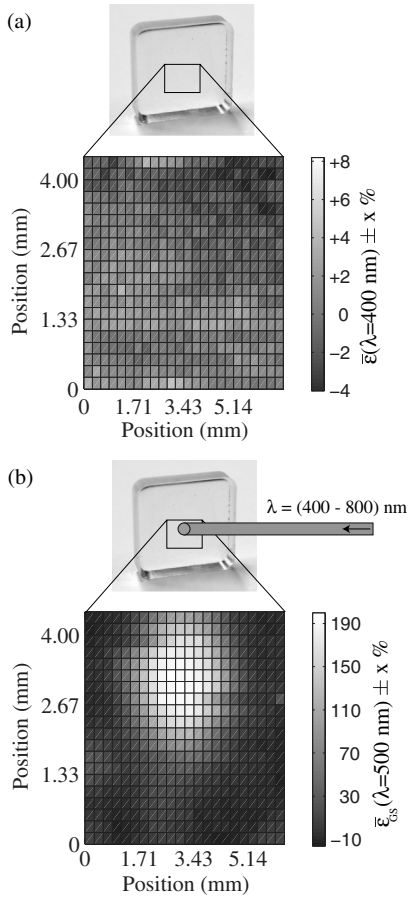

Fig. 5. (a) Spatial homogeneity of the extinction coefficient ε at $\lambda = 400$ nm in top view of a 3D OSO-PDMS sample and related to its average value. (b) ε at $\lambda = 500$ nm after illumination of a dot with a diameter of 2.6 mm.

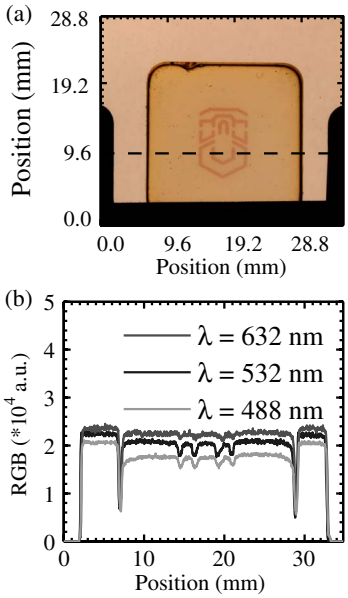

Fig. 6. (a) Emblem of the Osnabrück University being illuminated in an OSO-PDMS sample. (b) Transmitted light intensity for the wavelengths $\lambda = (632 \pm 10)$ nm, $\lambda = (532 \pm 10)$ nm, and $\lambda = (488 \pm 10)$ nm at the dashed line in (a).

extinction feature of the isomers in the green spectral range) become visible.

In Fig. 6(b) the spectral bandwidth of the white-light source is narrowed to characteristic RGB colors of $\lambda = (632 \pm 5)$ nm, $\lambda = (532 \pm 5)$ nm, and $\lambda = (488 \pm 5)$ nm via appropriate interference filters. Then the transmitted light intensity is plotted along the dashed line in Fig. 6(a). From these data, the spectral contrast C can be determined individually for the three colors from the maximum amplitude of the transmission change that yields a ratio of $C_R : C_G : C_B = 0.48 : 1 : 0.92$. The same data can be applied for the determination of the contour sharpness Δm of the image from the gradient of the transmission slope. Here, we get $\Delta m_R : \Delta m_G : \Delta m_B = 0.62 : 1 : 0.92$, that is, the samples features sufficient values of both spectral contrast and contour sharpness over the visible spectral range.

Now the optical resolution of an OSO-PDMS sample is analyzed in view of an application in high-density optical storage. Therefore, a resolution test mask of 1951 USAF (see Fig. 7) and a monochromatic light source at $\lambda = 405$ nm is applied for image recording.

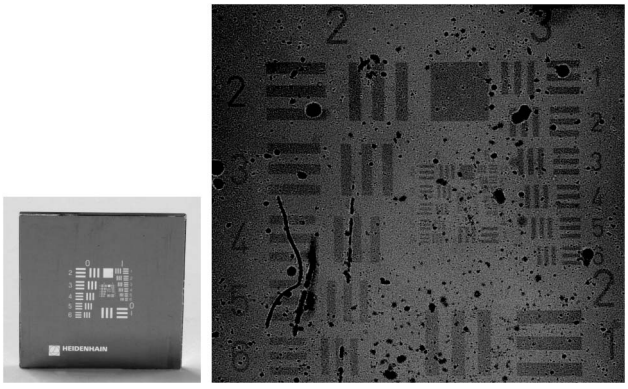

Fig. 7. Structures of a 1951 USAF target are transferred into an OSO-PDMS sample and analyzed by a microscope.

The microscopic photograph of the recorded image shows the recorded structures in the sample, indicated by the darker color of the metastable states. By comparison with the resolution chart of the mask, an optical resolution of more than 16 μm is verified without losses in the contrast. The independency of the contrast as a function of spatial frequency down to the nanometer scale results from the photofunctionality of the PDMS sample on the molecular level.

4. CONCLUSION

Concluding these results, this paper illustrates the successful embedding of molecular ruthenium sulfoxide compounds in a solid dielectric environment as a conceptually novel design of nonlinear optical materials. Contrary to the embedding of other transition-metal compounds the photofunctional properties are preserved. The studies have shown that compared to experiments in solution the spectral extinction change due to light exposure is only slightly affected. Furthermore, the relaxation times from the metastable structural isomers back to the ground state are increased in the order of 10^2 from several minutes up to hours after embedding in PDMS. With regard to an application, it is shown that the ruthenium sulfoxide compound OSO in the polymer PDMS offers a high-contrast, high-contour sharpness and a high optical resolution within the visible spectral range. This underlines the impact of OSO-PDMS as a material for high-density (holographic) data storage and display technologies.

APPENDIX A: SAMPLE PREPARATION

PDMS (Sylgard 184) is purchased from Dow Corning. It consists of two reagents, the prepolymer and the curing agent, which are confounded at a ratio of 1:5. DCM from Sigma Aldrich is used to solve the ruthenium sulfoxide compounds, which are synthesized at the Ohio University in the group of J. J. Rack. To evaporate the solvent and to produce a condensed PDMS structure, the sample is heated up to a specific temperature of 60°C for about 70 min. A reference sample is prepared using the same procedure but without the molecular sulfoxide compound. Typical concentrations of the molecular ruthenium sulfoxide compound in PDMS are on the order of $c = 0.3$ mmol $l^{-1} = 0.3$ mM.

APPENDIX B: EXPERIMENTAL METHODS

A two-beam spectrometer Shimadzu UV-3600 is used for absorption measurements. For temperature-dependent measurements, the sample holder in the Shimadzu spectrometer is modified with a Peltier stack. Two additional linear translation stages (Newport, AG-LS25) facilitate the possibility to analyze the sample in two dimensions in equidistant steps in the spectrometer. To obtain the extinction spectra for the μ-metastable structural isomers, the sample is illuminated by white light of a Zeiss KL 1500 LCD, emitting light in the spectral range of $\lambda = 400$–800 nm with an average intensity $I_{wl} \approx 25$ mW cm^{-2}. The digital photocamera (Canon EOS 10D) detects the transmitted light of the sample. For experiments with monochromatic light, a Coherent Cube 405 laser at the wavelength $\lambda = 405$ nm is used with an intensity of $I = 1$ mW cm^{-2} and exposure times of $t = 3$ h. Experiments with a microscope are realized with the Leica DM5000 B and 2.5-fold magnification. In addition, an interference filter

for $\lambda = (532 \pm 5)$ nm is used to increase the contrast in the microscope.

ACKNOWLEDGMENTS

This work was financially supported by the Deutsche Forschungsgemeinschaft (project INST 190/137-1) and the Ministry of Science and Culture of Lower Saxony (MWK). We also thank J. J. Rack from Ohio University for providing the ruthenium sulfoxide compounds.

REFERENCES

1. P. Gütlich, Y. Garcia, and Th. Woike, "Photoswitchable coordination compounds," Coord. Chem. Rev. **219**, 839–879 (2001).
2. D. Schaniel, M. Imlau, T. Weisemöller, T. Woike, K. W. Kramer, and H. U. Gudel, "Photoinduced nitrosyl linkage isomers uncover a variety of unconventional photorefractive media," Adv. Mater. **19**, 723–726 (2007).
3. M. Imlau, S. Haussühl, T. Woike, R. Schieder, V. Angelov, R. A. Rupp, and K. Schwarz, "Holographic recording by excitation of metastable electronic states in $Na_2Fe(CN)_5NO.2H_2O$ a new photorefractive effect," Appl. Phys. B **68**, 877–885 (1999).
4. P. Günter and J.-P. Huignard, *Photorefractive Materials and Their Applications 1* (Springer, 2006).
5. N. Ishii, T. Kato, and J. Abe, "A real-time dynamic holographic material using a fast photochromic molecule," Sci. Rep. **2**, 819–823 (2012).
6. F. K. Bruder, R. Hagen, T. Rolle, M. S. Weiser, and T. Facke, "From the surface to volume: concepts for the next generation of optical-holographic data-storage materials," Angew. Chem., Int. Ed. Engl. **50**, 4552–4573 (2011).
7. M. Imlau, T. Woike, S. Odoulov, and T. Bieringer, "Holographic data storage," in *Nanoelectronics and Information Technology*, R. Waser, ed. (Wiley-VCH, 2012), pp. 727–750.
8. V. Dieckmann, S. Eicke, K. Springfeld, and M. Imlau, "Transition metal compounds towards holography," Materials **5**, 1155–1175 (2012).
9. S. Haussühl, G. Schetter, and T. Woike, "Nitroprussides, a new group of materials for holographic information-storage on the basis of metastable electronic states," Opt. Commun. **114**, 219–222 (1995).
10. P. Coppens, D. V. Fomitchev, M. D. Carducci, and K. Culp, "Crystallography of molecular excited states: transition-metal nitrosyl complexes and the study of transient species," J. Chem. Soc. Dalton Trans. (6), 865–872 (1998).
11. D. Schaniel, J. Schefer, M. Imlau, and T. Woike, "Light-induced structural changes by excitation of metastable states in $Na_2[Fe(CN)_5NO]\cdot 2H_2O$ single crystals," Phys. Rev. B **68**, 104108 (2003).
12. J. M. Cole, "Applications of photocrystallography: a future perspective," Z. Kristallogr. **223**, 259–271 (2008).
13. T. Woike and D. Schaniel, "Photocrystallography," Z. Kristallogr. **223**, 4–5 (2008), Special Issue.
14. D. H. Close, A. D. Jacobson, J. D. Margerum, R. G. Brault, and F. J. McClung, "Hologram recording on photopolymer materials," Appl. Phys. Lett. **14**, 159–160 (1969).
15. M. Irie, "Photoresponsive polymers," Adv. Polym. Sci. **94**, 27–67 (1990).
16. P. H. Rasmussen, P. S. Ramanujam, S. Hvilsted, and R. H. Berg, "A remarkably efficient azobenzene peptide for holographic information storage," J. Am. Chem. Soc. **121**, 4738–4743 (1999).
17. A. Shishido, "Rewritable holograms based on azobenzene-containing liquid-crystalline polymers," Polymer J. **42**, 525–533 (2010).
18. N. G. Shimkina, M. M. Krayushkin, V. A. Barachevsky, A. A. Dunaev, B. A. Izmailov, V. A. Vasnev, and M. L. Keshtov, "Photochromic silicone polymers based on 1,2-dihetarylethenes," ARKIVOC **iv**, 112–119 (2008).
19. V. Dieckmann, M. Imlau, D. H. Taffa, L. Walder, R. Lepski, D. Schaniel, and T. Woike, "Phototriggered NO and CN release from [Fe(CN)(5)NO](2-) molecules electrostatically attached to TiO2 surfaces," Phys. Chem. Chem. Phys. **12**, 3283–3288 (2010).
20. A. Schuy, T. Woike, and D. Schaniel, "Photoisomerisation in single molecules of nitroprusside embedded in mesopores of xerogels," J. Sol. Gel Sci. Technol. **50**, 403–408 (2009).
21. J. J. Rack, "Electron transfer triggered sulfoxide isomerization in ruthenium and osmium complexes," Coord. Chem. Rev. **253**, 78–85 (2009).
22. V. Dieckmann, S. Eicke, J. J. Rack, Th. Woike, and M. Imlau, "Pronounced photosensitivity of molecular $[Ru(bpy)_2(OSO)]^+$ solutions based on two photoinduced linkage isomers," Opt. Express **17**, 15052–15060 (2009).
23. D. P. Butcher, A. A. Rachford, J. L. Petersen, and J. J. Rack, "Phototriggered S→O isomerization of a ruthenium-bound chelating sulfoxide," Inorg. Chem. **45**, 9178–9180 (2006).
24. M. J. Root and E. Deutsch, "Synthesis and characterization of (bipyridine)(terpyridine)(chalcogenoether)ruthenium(ii) complexes—kinetics and mechanism of the hydrogen-peroxide oxidation of $[(bpy)(tpy)RuS(CH_3)_2]^{2+}$ to $[(bpy)(tpy)RuS(O)(CH_3)_2]^{2+}$—kinetics of the aquation of $[(bpy)(tpy)RuS(O)(CH_3)_2]^{2+}$," Inorg. Chem. **24**, 1464–1471 (1985).
25. J. N. Lee, C. Park, and G. M. Whitesides, "Solvent compatibility of poly(dimethylsiloxane)-based microfluidic devices," Anal. Chem. **75**, 6544–6554 (2003).
26. T. A. Grusenmeyer, B. A. McClure, C. J. Ziegler, and J. J. Rack, "Solvent effects on isomerization in a ruthenium sulfoxide complex," Inorg. Chem. **49**, 4466–4470 (2010).
27. S. Eicke, V. Dieckmann, A. Kruse, K.-M. Voit, M. Imlau, and L. Walder, "Dynamics of the light-induced absorption in photochromic $[Ru(bpy)_2(OSO)]^+$," J. Spectrosc. Dyn. (to be published).
28. V. Dieckmann, K. Springfeld, S. Eicke, M. Imlau, and J. J. Rack, "Thermal stability, photochromic sensitivity and optical properties of $[Ru(bpy)_2(OSOR)]^+$ compounds with R = Bn, BnCl, BnMe," Opt. Express **18**, 23495–23503 (2010).